Low-energy nuclear reaction of the $^{14}N + ^{169}Tm$ system: Incomplete fusion

R. Kumar,[1] Vijay R. Sharma,[1,*] Abhishek Yadav,[1] Pushpendra P. Singh,[2] Avinash Agarwal,[3] S. Appannababu,[4] S. Mukherjee,[5] B. P. Singh,[6] R. Ali,[7] and R. K. Bhowmik[1]

[1]*Nuclear Physics Group, Inter-University Accelerator Center, New Delhi 110 067, India*
[2]*Department of Physics, Indian Institute of Technology Ropar, Rupnagar, Punjab 140 001, India*
[3]*Physics Department, Bareilly College, Bareilly 243 005, India*
[4]*Departamento de Fisica Nuclear, Instituto de Fisica, Universidade de Sao Paulo, CEP 05508 090, Brazil*
[5]*Physics Department, Maharaja Sayajirao University of Baroda, Vadodara 390 002, India*
[6]*Accelerator Laboratory, Department of Physics, A. M. University, Aligarh 202 002, India*
[7]*Department of Physics, Gandhi Faiz-E-Aam (Post Graduate) College, Shahjahanpur 242 001, India*

(Received 19 May 2017; revised manuscript received 16 August 2017; published 30 November 2017)

Excitation functions of reaction residues produced in the $^{14}N + ^{169}Tm$ system have been measured to high precision at energies above the fusion barrier, ranging from $1.04V_B$ to $1.30V_B$, and analyzed in the framework of the statistical model code PACE4. Analysis of α-emitting channels points toward the onset of incomplete fusion even at slightly above-barrier energies where complete fusion is supposed to be one of the dominant processes. The onset and strength of incomplete fusion have been deduced and studied in terms of various entrance channel parameters. Present results together with the reanalysis of existing data for various projectile-target combinations conclusively suggest strong influence of projectile structure on the onset of incomplete fusion. Also, a strong dependence on the Coulomb effect ($Z_P Z_T$) has been observed for the present system along with different projectile-target combinations available in the literature. It is concluded that the fraction of incomplete fusion linearly increases with $Z_P Z_T$ and is found to be more for larger $Z_P Z_T$ values, indicating significantly important linear systematics.

DOI: 10.1103/PhysRevC.96.054614

I. INTRODUCTION

In recent years, widespread experimental and theoretical efforts have been made to understand the onset and dynamics of massive transfer events in incomplete fusion (ICF) reactions at low incident energies (i.e., ≈4–7 MeV/nucleon) [1–11]. Massive transfer events, where only a part of projectile fuses with the target nucleus, were first identified in heavy-ion induced reactions by Britt and Quinton [12] during the bombardment of ^{197}Au and ^{209}Bi with ^{12}C, ^{14}N, and ^{16}O beams at $E_{lab} \approx 7$–10 MeV/nucleon. Since then, a variety of dynamical models and theories have been proposed to understand the production of massive transfer events [13–18]; see Refs. [8,19] for detailed descriptions. Udagawa and Tamura [14], in their breakup fusion model (BUF), described ICF as two-step process. According to the BUF model, the incident projectile breaks up into its constituent clusters, e.g., ^{12}C may break up in to $^{8}\mathrm{Be} + \alpha$ or $\alpha + \alpha + \alpha$. One of these fragments may fuse with the target nucleus to form an incompletely fused composite system, and the remnant is emitted at forward angles with an energy $E_{\mathrm{remnant}} = E_{\mathrm{proj.}} \times A_{\mathrm{remnant}}/A_{\mathrm{proj.}}$. The concept of fractional linear momentum transfer in ICF events has been emphasised in the velocity distributions of heavy recoils, where more than one linear momentum component has been observed in the $^{16}O + ^{169}Tm$ system [9]. On the other hand, Tserruya *et al.* [20] showed the onset of ICF below the critical angular momentum limit (ℓ_{crit}) for complete fusion (CF). Apart from the well documented existence of low energy ICF (see Refs. [4–10] for details), no satisfactory picture has emerged to explain ICF data obtained at relatively lower projectile energies, i.e., starting from the Coulomb barrier to $1.40V_B$. At these energies, CF is supposed to be one of the major contributors to the reaction cross-section [21]. However, a substantial fraction of ICF has been observed even at slightly above-barrier energies [4,10,22–24], and has been justified in terms of driving angular momenta imparted into the system due to peripheral interactions at large impact parameters [1,7,25,26]. Further, Morgenstern's mass-asymmetry systematics [27] has been supplemented [24] by Singh *et al.*, indicating that the ICF fraction increases with entrance channel mass asymmetry for individual projectiles only [24]. Note that the conclusions drawn in Refs. [24] are based on the results obtained with α-cluster beams (e.g., ^{12}C, ^{16}O). The α-cluster beams may break up into constituent α clusters which may lead to population of more ICF channels. Nevertheless, how ICF shows up for $1n/2n/1p/2p/1pn$ excess beams, when compared to ^{12}C and ^{16}O projectiles, is an open and interesting question. For better insights into the onset and strength of ICF in terms of various entrance channel parameters, inclusive measurements are planned with beams of ^{13}C, ^{14}N, and ^{18}O on a ^{169}Tm nucleus.

The present work is an extension of our earlier measurements to study the effect of ^{12}C projectiles with neutron and proton excess on ICF reaction dynamics. The excitation functions (EFs) of individual evaporation residues produced in the $^{14}N + ^{169}Tm$ system have been measured and analyzed within the framework of statistical model code PACE4 based on equilibrated compound nucleus (CN) decay. The ICF strength function is deduced from the analysis of experimental EFs.

*Corresponding author: phy.vijayraj@gmail.com

Findings of present measurements have been compared with those obtained using α-clustered beams (^{12}C, ^{16}O). The effect of an additional np pair over the α-cluster configuration of a ^{12}C beam [i.e, ^{14}N = $3\alpha(^{12}\mathrm{C}) + pn$] on the onset and strength of ICF has been investigated in terms of projectile structure and charge dependence on projectile as well as target.

This paper is organized as follows: Experimental procedures are given in Sec. II, and the results and their interpretations in context with statistical model code PACE4 are presented in Sec. III. The influence of ICF on CF and its dependence on various entrance channel parameters is demonstrated in Sec. IV. Section V deals with the summary and conclusions of the present work.

II. EXPERIMENTAL PROCEDURES

In the present experiment, a beam of ^{14}N was provided by the 15UD Pelletron accelerator of the Inter-University Accelerator Centre (IUAC), New Delhi, at four bombarding energies, i.e., $E_{\mathrm{lab}} \approx 83, 80, 78$, and 76 MeV, with am intensity of 25 to 30 nA. To cover a wide energy range in an irradiation, an energy degradation technique was used. Self-supporting natural ^{169}Tm (abundance 100%) target foils of thicknesses 1.2 to 1.7 mg/cm^2 were prepared by rolling technique. In order to trap recoiling products during the irradiations, Al catcher foils of thicknesses 1.1 to 2.0 mg/cm^2 were placed downstream from the target foil. In this experiment, five stacks (each made by two to three target-catcher foil assemblies) were irradiated to achieve at least 12 energy points. The incident beam energy on each target foil in a stack was estimated using the code SRIM [28]. For example, at the highest incident energy the uncertainty in the energy due to finite sample thickness is estimated to be $\pm$0.84 MeV. The uncertainty in the projectile energy is indicated in the figures as well.

Irradiations were performed in the General Purpose Scattering Chamber (GPSC) for a duration of $\approx$8–12 hours for each stack. The beam flux was calculated using the total charge collected in the Faraday cup installed behind the stack assembly. In order to minimize the lapse time between stop of the irradiation and beginning of the counting, an in-vacuum transfer facility was employed to take out the stack assemblies after irradiations. The radioactivity produced in each target-catcher assembly was measured offline for several days with two high resolution high-purity germanium (HPGe) detectors. The HPGe detectors were precalibrated for efficiency and energy using standard γ sources at various source-detector separations to avoid solid-angle effects during the offline counting.

III. DATA REDUCTION, RESULTS, AND THEIR INTERPRETATIONS

The reaction residues have been identified by their characteristic γ lines, and are further confirmed by decay-curve analysis. A typical γ-ray spectrum obtained at $E_{\mathrm{lab}} = 82.16 \pm 0.84$ MeV is shown in Fig. 1. In this figure, the γ peaks corresponding to different evaporation residues are labeled. Reaction residues identified in the present work and their spectroscopic data are given in Table I. Note that ERs having

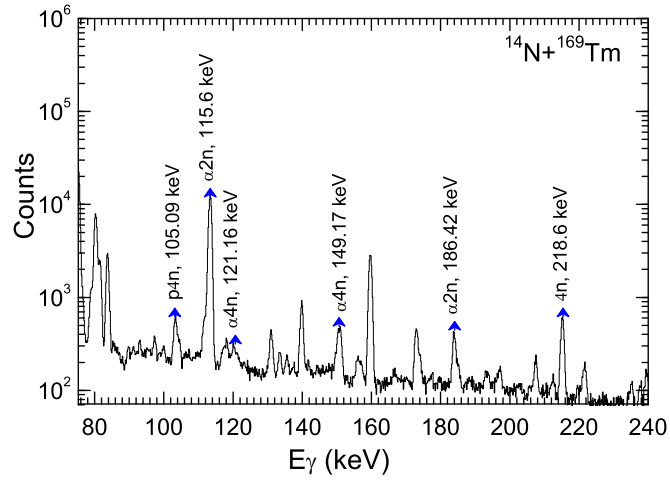

FIG. 1. Typical γ-ray spectra obtained for the $^{14}\mathrm{N} + {}^{169}\mathrm{Tm}$ system at $E_{\mathrm{lab}} = 82.16 \pm 0.84$ MeV. γ peaks indicating CF and/or ICF residues are marked by arrows.

$T_{1/2} < 5$ min and $T_{1/2} > 18$ h have not been identified due to experimental limitations. The absolute production cross sections of evaporation residues [$\sigma_r(E)$] have been deduced using the standard formulation [9].

The errors in experimentally measured residue cross-sections may arise mainly due to the (i) nonuniform thickness of target foils, (ii) fluctuations in the beam current, and (iii) error in efficiency and dead time of the HPGe detector. The overall errors from the aforementioned factors including statistical errors are estimated to be $\leqslant$15% [29]. Note that the quoted errors exclude uncertainty in nuclear data, such branching ratio, decay constant, etc., which have been taken from the *Table of Isotopes* [30].

In the present work, the experimental EFs of ^{179}Os ($4n$), ^{179}Re ($p3n$), ^{178}Re ($p4n$), ^{177}W ($\alpha 2n$), ^{176}W ($\alpha 3n$), ^{175}W ($\alpha 4n$), and ^{174}W($\alpha 5n$) evaporation residues have been analyzed in the framework of equilibrated CN decay using statistical model code PACE4 [31]. A short account of PACE4 is given in the next section for ready reference.

A. Analysis of EFs with PACE4

The code PACE4 is based on the Hauser-Feshbach approach of CN deexcitation [31]. The production crosssections of evaporation residues are calculated using the Bass formula

TABLE I. Identified evaporation residues with their spectroscopic properties produced in the $^{14}\mathrm{N} + {}^{169}\mathrm{Tm}$ system via CF and/or ICF.

Residue(s)	$t_{1/2}$	Spin	E_γ (keV)	I_γ
^{179}Os($4n$)	6.5 min	$1/2^-$	218.6, 593.8	4.89, 4.52
^{179}Re($p3n$)	19.5 min	$5/2^+$	189.05, 289.97	7.5, 26.9
^{178}Re($p4n$)	13.2 min	3^+	105.9, 237.3	23.0, 45
^{177}W($\alpha 2n$)	132 min	$1/2^-$	115.6, 426.98	51, 13.2
^{176}W($\alpha 3n$)	2.5 h	0^+	100.20	18
^{175}W($\alpha 4n$)	35.2 min	$1/2^-$	121.16, 149.17	1.8, 149.17
^{174}W($\alpha 5n$)	33.2 min	0^+	328.68, 428.83	9.5, 12.7

[32], and the deexcitation of CN is followed by a Monte Carlo procedure. The projections of angular momentum are calculated at each stage of deexcitation, which enables the determination of angular distribution of light nuclear particles (LNPs) emitted during the deexcitation of the CN. The optical model potentials of Becchetti and Greenlees [33] are used to calculate transmission coefficients for neutrons and protons, and the optical model potential of Satchler [34] is used to calculate α particle emissions. The partial cross section (σ_ℓ) for the formation of CN at angular momentum ℓ and specific bombarding energy E is given by

$$\sigma_\ell = \frac{\lambda^2}{4\pi}(2\ell+1)T_\ell. \quad (1)$$

Here, λ is reduced the wavelength. The transmission coefficients T_ℓ may be given as

$$T_\ell = \left[1+\exp\left(\frac{\ell-\ell_{\max}}{\Delta}\right)\right]^{-1}. \quad (2)$$

In Eq. (2), Δ is the diffuseness parameter and $\ell_{\max}$ is the maximum value of ℓ obtained by the total fusion cross section,

$$\sigma_F = \sum_{\ell=0}^{\infty}\sigma_\ell. \quad (3)$$

The transmission coefficients for the evaporation of LNPs (n, p, and α) during the deexcitation of excited CN are obtained by optical model calculations. The fission decay mode may be considered using a rotating liquid drop fission barrier routine. In this code, the level density parameter a ($=A/K$) is one of the important input parameters, where A is the mass number of the nucleus and K is a free parameter. The value of K may be varied to reproduce experimental excitation functions within the physical limits.

1. xn, pxn channels

Experimental EFs of ^{179}Os($4n$), ^{179}Re($p3n$), and ^{178}Re($p4n$) evaporation residues are compared with the predictions of statistical model code PACE4. In order to reproduce experimental EFs of xn/pxn channels, different values of level density parameter from $A/8$ to $A/10$ MeV^{-1} were tested. Figure 2 shows the comparison of experimentally measured and theoretically calculated EFs of xn/pxn channels. As shown in this figure, the experimental EFs of xn/pxn channels are very well reproduced by statistical model code PACE4 for the level density parameter $a = A/8$ MeV^{-1} for the studied energy range within the experimental uncertainties. This confirms the population of ^{179}Os($4n$), ^{179}Re($p3n$), and ^{178}Re($p4n$) residues via CF of ^{14}N with ^{169}Tm followed by emission of LNPs from the excited compound nucleus ^{183}Os*. As a representative case, the population of ^{179}Os is as follows:

$$^{14}\mathrm{N} + {}^{169}\mathrm{Tm} \Rightarrow ({}^{183}\mathrm{Os}^\star) \Rightarrow {}^{179}\mathrm{Os} + 4n.$$

The agreement of PACE4 predictions with experimentally measured excitation functions displayed in Fig. 2 reflects a suitable choice of level density parameter for the studied energy range. Therefore, the value of $a = A/8$ MeV^{-1} can be used as a fixed parameter for the analysis of α-emitting

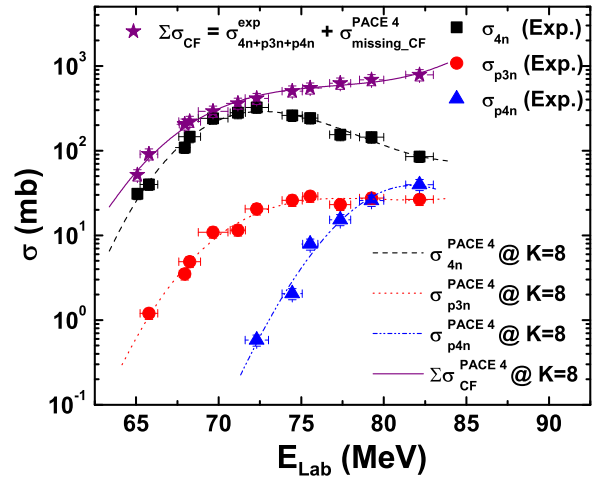

FIG. 2. Comparison of experimental and theoretical EFs of xn/pxn channels. Dashed and solid line(s) drawn through the data points represent best fits to the PACE4 predictions for level density parameter $a = A/8$ MeV^{-1}.

channels expected to have contribution from both CF and ICF. The same value of level density parameter was suggested by Gilbert and Cameron [35] for the studied energy range in this mass region. Since PACE4 does not take ICF into account, any enhancement in the experimental EFs over PACE4 predictions (for a level density parameter $a = A/8$ MeV^{-1}) may be attributed to ICF.

Further, it note that the ^{14}N projectile has less negative proton separation energy (7.55 MeV) than α separation energy (11.61 MeV). This clearly indicates a more favorable breakup channel than α breakup, where ^{14}N may break into ^{13}C + p and where ^{13}C may fuse with ^{169}Tm forming a ^{182}Re* composite system and a proton moving in the forward direction as a spectator. The reduced excited compound nucleus ^{182}Re* decays through the emission of 3 or 4 neutrons. However, no such observation has been made experimentally in proton emitting channels.

Furthermore, in order to test the accuracy in our measurements, an attempt has been made to deduce the value of the fusion barrier (V_B) using the classical prescription given by Gutbrod *et al.* [36]. The formula for fusion the cross section is

$$\sigma_{\mathrm{CF}} = \pi R^2_{\mathrm{int.}}(1 - V_B/E_{\mathrm{lab}}). \quad (4)$$

Since the experimentally measured complete fusion cross section matches with compound nucleus decay based on statistical model code PACE4, the normalized values of σ_{CF} (corrected for missing channels; see Fig. 2) is plotted as a function of $1/E_{\mathrm{lab}}$ in Fig. 3. As shown in this figure, the data points follow a straight line which intersects the x axis at E_{lab} corresponding to 63 MeV with an uncertainty of 2%, which reproduces the calculated fusion barrier of the ^{14}N + ^{169}Tm system and gives confidence in our measurements [4].

2. αxn channels

In Fig. 4(a), experimental EFs of ^{177}W ($\alpha 2n$, $T_{1/2} = 2.2$ h), ^{176}W ($\alpha 3n$, $T_{1/2} = 2.5$ h), ^{175}W ($\alpha 4n$, $T_{1/2} = 35.2$ min),

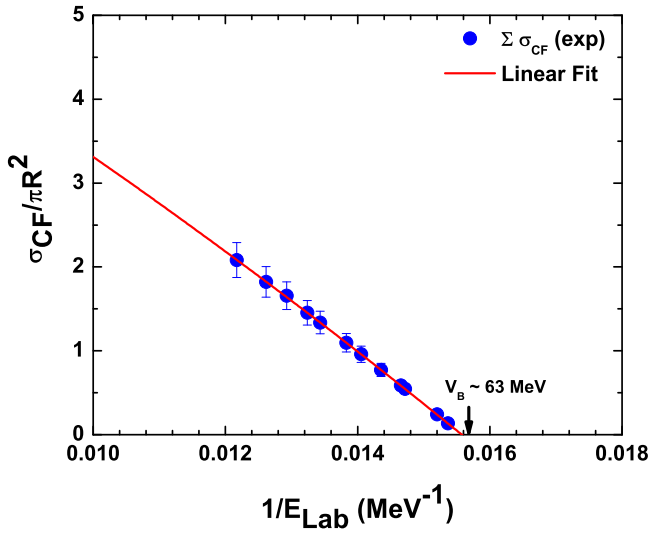

FIG. 3. CF cross sections as a function of $1/E_{\rm lab}$ found to reproduce the Coulomb barrier for ^{14}N + ^{169}Tm system. The dashed line through the data points is achieved by a best-fitting procedure on the data.

and ^{174}W ($\alpha 5n$, $T_{1/2} = 33.2$ min) evaporation residues are compared with PACE4 predictions using the same set of input parameters that were used to reproduce CF channels. Dotted lines through data points are drawn to guide the eyes. On the other hand, cross sections for $\alpha 2n$, $\alpha 3n$, $\alpha 4n$, and $\alpha 5n$ via statistical code PACE4 are indicated with self-explanatory notation in Fig. 2(a). Note that ICF is not taken into consideration in PACE4; therefore, calculation of cross sections for α-emitting channels with this code may illuminate the underlying physical effects. As can be seen in Fig. 4(a), the experimental EFs of $^{177-174}$W are significantly enhanced as compared to the PACE4 predictions for the studied energy range. The enhancement in experimental EFs over PACE4 predictions may be attributed to the ICF processes. In order to account for the enhanced cross sections in the studied α-emitting channels, the sum of all α-emitting channels is compared with that predicted by PACE4 in Fig. 4(b). As can be seen in Fig. 4(b), the experimental EF(s) of α-emitting channel(s) ($\sum \sigma_{\alpha xn}$) are found to be significantly enhanced compared to that predicted by PACE4 (blue solid line). This enhancement may be attributed to the contribution from ICF. Therefore, the evaporation residues ^{177}W ($\alpha 2n$), ^{176}W ($\alpha 3n$), ^{175}W($\alpha 4n$), and ^{174}W ($\alpha 5n$) are assumed to be populated via both CF and ICF by following different decay chains:

(i) Complete fusion: ^{14}N fuses with a ^{169}Tm nucleus to form an ^{183}Os* nucleus which may eventually emit an α particle and a few (x) neutrons to reach W isotopes:

$$^{14}\mathrm{N} + {}^{169}\mathrm{Tm} \Rightarrow {}^{183-\alpha}\mathrm{Os}^{\star} \Rightarrow {}^{179}\mathrm{W}$$
$$\Rightarrow {}^{179-xn}\mathrm{W} + \alpha xn \quad (\text{here } x = 2\text{–}5).$$

(ii) Incomplete fusion: Only a part of ^{14}N (for instance ^{10}Be) fuses with the ^{169}Tm nucleus to form a reduced CN ^{179}W*, and the remnant α cluster (^{4}He) is emitted as a spectator. The excited ^{179}W* nucleus emits a few (x) neutrons to give rise to final reaction products:

$$^{14}\mathrm{N}(^{10}\mathrm{Be} + \alpha) \Rightarrow {}^{10}\mathrm{Be} + {}^{159}\mathrm{Tm} \Rightarrow {}^{179}\mathrm{W}^{\star}$$
$$\Rightarrow {}^{179-xn}\mathrm{W} + xn + \alpha \quad (\alpha \text{ as a spectator}).$$

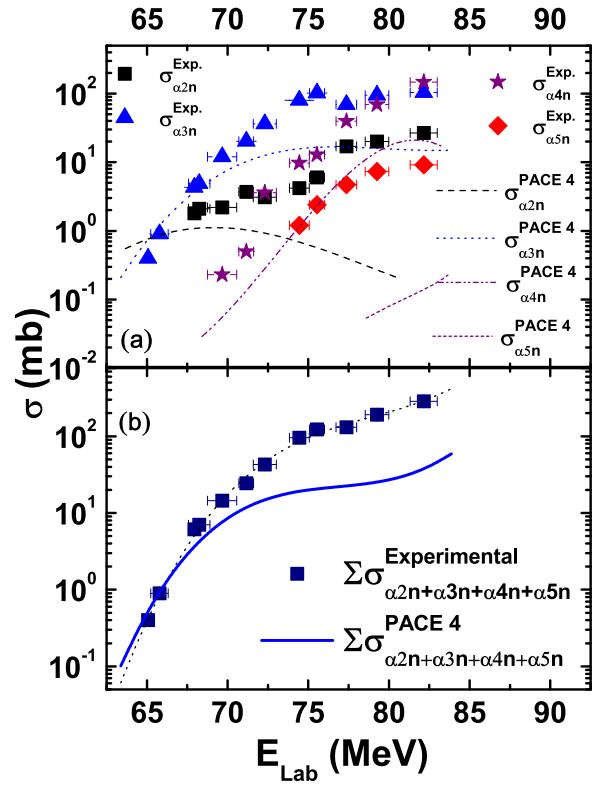

FIG. 4. (a) Experimentally measured EFs of ERs ^{177}W ($\alpha 2n$), ^{176}W ($\alpha 3n$), ^{175}W ($\alpha 4n$), and ^{174}W ($\alpha 5n$) are compared with the PACE4 predictions at level density parameter $K = 8$. (b) The dashed line through the experimental data points is the best fit to the sum of all experimentally measured αxn channels ($\sum \sigma_{\alpha} xn$), and the solid line represents PACE4 prediction for $K = 8$ for these channels.

The relative strengths of CF and ICF in an α-emitting channel were deduced as suggested by Gomes *et al.* [37]. The ICF fraction was accounted for by subtracting CF cross sections ($\sigma^{\rm PACE4}$) from the experimentally measured cross sections ($\sigma^{\rm exp}$) at respective projectile energies. Note that Gasques *et al.* [38] in their study of ^{10,11}B + ^{209}Bi used a reaction ^{30}Si + ^{186}W [39], where no ICF contribution was expected due to the nature of the projectiles [40]. This is an alternative approach [38] to understanding the complete and incomplete fusion dynamics in heavy-ion reactions. However, the present experiment was planned to probe the existence of incomplete fusion in the ^{14}N + ^{169}Tm system at low incident energies. Note that the complete and incomplete fusion events can be clearly identified in recoil range distribution measurements. In Refs. [4,8,9,41] the relative contributions of CF and ICF deduced from the analysis of recoil range distributions have been found to be in good agreement with those obtained from the analysis of excitation functions in the framework of theoretical model code PACE4, a methodology

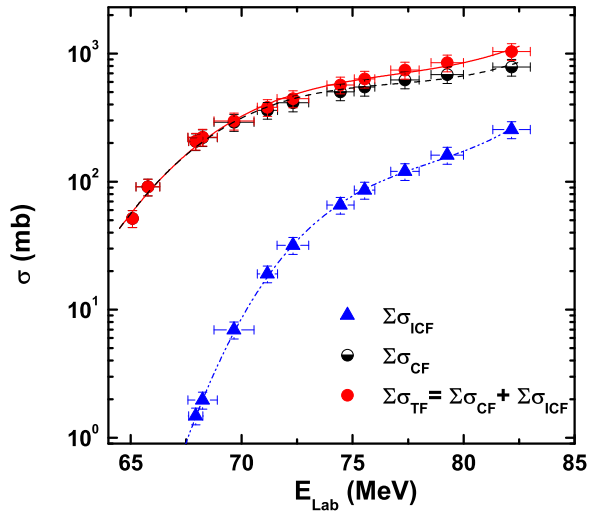

FIG. 5. Total fusion probability ($\sum\sigma_{TF}$) is plotted with the sum of all CF ($\sum_{CF}$) and ICF ($\sum\sigma_{ICF}$) channels. Increasing separation between $\sum\sigma_{TF}$ and $\sum\sigma_{CF}$ with incident projectile energy reflects the ICF fraction. Lines and curves are drawn to guide the eyes.

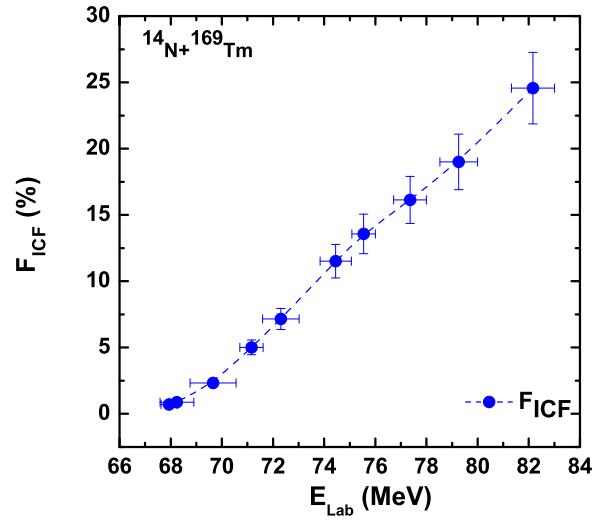

FIG. 6. The ICF strength function for the ^{14}N + ^{169}Tm system (see text for description). Lines are drawn to guide the eyes.

used in the present work. This suggests that the code PACE4 may be used to determine the ICF contribution in α-emitting channels in the energy range of interest.

In order to demonstrate the contribution of ICF to total fusion (given as $\sigma_{TF} = \sum\sigma_{CF} + \sum\sigma_{ICF}$) at various incident energies, the value of σ_{TF} is compared with $\sum\sigma_{ICF}$ and $\sum\sigma_{CF}$ in Fig. 5. The lines through the data points are drawn to guide the eyes. In this figure, the increasing separation between $\sum\sigma_{CF}$ and $\sum\sigma_{TF}$ with incident energy suggests strong energy dependence of ICF. The ICF shows significant contribution to $\sum\sigma_{CF}$ even at slightly above-barrier energies, and smoothly increases for higher incident energies. Observation of large ICF fraction at higher incident energies can be correlated with the breakup probability of the incident ion, which depends on input angular momenta imparted into the system by means of bombarding energy and/or due to higher values of impact parameters.

B. Onset and strength of incomplete fusion

For better insights into the onset and strength of ICF, the percentage fraction of ICF (F_{ICF}), which is the measure of ICF strength at a particular energy, has been deduced from the analysis of data presented in Fig. 4. The value of F_{ICF} is given by the following expression:

$$F_{ICF} = \frac{\sum\sigma_{ICF}}{\sum\sigma_{CF+ICF}} \times 100. \quad (5)$$

The value of F_{ICF} for ^{14}N + ^{169}Tm system is plotted in Fig. 6 with incident energy; this is termed the ICF strength function. The ICF strength function defines the empirical probability of ICF at different incident energies. In Eq. (5), $\sum\sigma_{CF}$ is the sum of cross sections for all identified xn and pxn channels, with the corrections made for the missing channels via PACE4 predictions. As shown in Fig. 6, at the threshold of ICF (i.e., 67.94 ± 0.32 MeV) the value of F_{ICF} is found to be less than 1% of σ_{TF}, which increases at higher energies. At the highest studied energy (82.16 ± 0.84 MeV), the value F_{ICF} approaches nearly 24% of σ_{TF}. Similar dependence of ICF on incident energy has been noticed in Refs. [4,10] for different projectile-target combinations. Note that the present work has been carried out to explore the entrance channel effect on ICF fraction and to clarify the contradiction with Morgenstern's mass-asymmetry systematics [27]. In order to understand the entrance channel effect, the ICF strength function for ^{14}N + ^{169}Tm system is compared with that obtained for ^{12}C,^{16}O + ^{169}Tm systems in Fig. 7. In this figure, the ICF strength functions for non-α(^{14}N) and α-cluster

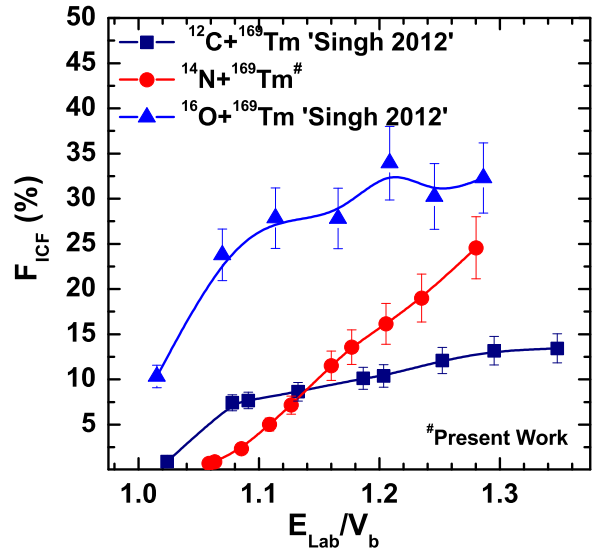

FIG. 7. The values of F_{ICF} obtained for ^{12}C,^{14}N,^{16}O + ^{169}Tm reactions are plotted as a function of normalized projectile energies. Lines drawn through the data points guide the eyes [24].

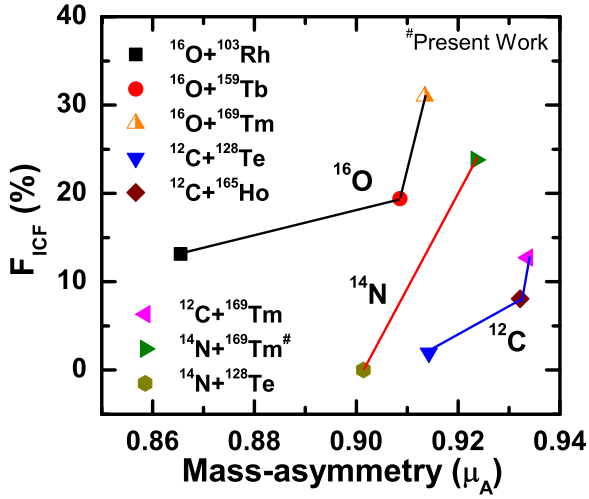

FIG. 8. The values of F_{ICF} for different projectile-target combinations as a function of entrance channel mass asymmetry (μ_A) at a constant relative velocity (i.e., $v_{\mathrm{rel}} = 0.053c$). The lines drawn through the data points guide the eyes for individual (^{12}C, ^{14}N, ^{16}O) projectiles.

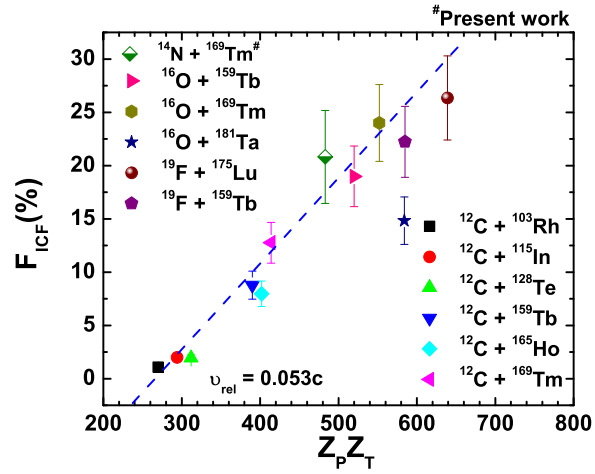

FIG. 9. Incomplete fusion strength function (F_{ICF}) of various systems (see text) as a function of Z_PZ_T. The dashed line is drawn to guide the eyes.

structure (^{12}C, ^{16}O) beams with the same ^{169}Tm target are plotted with normalized incident energy. The energy axis is normalized to incorporate the Coulomb barrier of given projectile-target combinations. As can be seen from this figure, the ICF contributes significantly even at slightly above-barrier energies. Further, the value of F_{ICF} is different for different beams at a constant normalized incident energy, which clearly reveals a projectile-structure/mass-asymmetry effect on ICF fraction.

In order to refine the aforementioned observation, the values of F_{ICF} for nearby systems are plotted with entrance channel mass asymmetry (μ_A) in Fig. 8 at a constant relative velocity ($v_{\mathrm{rel}} \approx 0.053c$). Lines through the data points are drawn to guide the eyes for individual projectiles. As can be seen from this figure, Morgenstern's mass-asymmetry systematic do not explain the variation of F_{ICF} with μ_A for the given projectile-target combinations. However, the value of F_{ICF} increases with μ_A for individual projectiles. One of the reasons for such behavior may be understood by considering that, for a given projectile, as the mass asymmetry increases the Coulomb effect (repulsion) also increases, giving rise to a larger breakup probability. Further, with the increase in projectile mass (charge) the breakup probability is expected to be more. As can be seen from Fig. 8, for the same value of mass asymmetry the projectile with higher charge has relatively higher breakup probability.

As demonstrated above, the onset and strength of ICF strongly depend on projectile type and projectile energy. Further, we extended this study in terms of charge dependence of ICF fraction. Therefore, to display the charge dependence of the ICF strength function for the presently studied system, the F_{ICF} values are plotted in Fig. 9 as a function of Z_PZ_T [i.e., the product of the projectile atomic number (Z_P) and the target atomic number (Z_T) of the system along with F_{ICF} of other systems available in the literature (see Refs. [4,10,42–44] for details) to show Z_PZ_T systematics, if any, at the same v_{rel} ($0.053c$). As can be seen from this figure, the percentage of incomplete fusion fraction F_{ICF} follows almost a linear growth as the charge product Z_PZ_T increases. Moreover, the value of F_{ICF} is found to be more for larger Z_PZ_T values, which indicates the role of Coulomb repulsion on ICF fraction; i.e., as the projectile comes near the field of the target nucleus (for higher Z_PZ_T) it may break up more easily compared to a low Z_PZ_T projectile-target combination. Hence, it may be concluded that an increase in the value of Z_PZ_T enhances the strength of the Coulomb interaction resulting in the larger breakup probability.

From the above findings, we report that the picture of ICF at energies starting from threshold to 7 MeV/nucleon is not very clear theoretically. However, the present experimental findings conclude clearly that projectile structure, projectile energy, and charge affect the onset and strength of ICF. This work may be helpful for the development of ICF dynamic modeling at low energies. Further, similar kinds of investigations are needed to support the present investigation of the ICF reaction process, particularly for a non-α-cluster beam.

IV. SUMMARY AND CONCLUSIONS

The present work reports the investigation of a nuclear reaction in terms of incomplete fusion processes. Seven reaction residues were identified. The cross sections of α exit channels were found to be enhanced when compared with the theoretical model using PACE4. Further, the strength of the ICF reaction has been deduced and an insight into the onset and strength of ICF as a function of incident energy, entrance channel mass asymmetry (μ_A), and charges of projectile as well as target was investigated. Existence of ICF at low incident energies has been conclusively demonstrated in the experimentally measured ICF strength function. It has been found that the value of F_{ICF} increases with incident energy. A comparison of F_{ICF} for different projectile-target combinations displays higher ICF probability for the $^{16}\mathrm{O} + ^{169}\mathrm{Tm}$ system, though

it is a less mass-asymmetric system than $^{12}C, ^{14}N + ^{169}Tm$ systems. Morgenstern's mass-asymmetry systematics do not explain the experimental data of eight nearby systems as a whole. However, the value of F_{ICF} is found to increase with entrance channel mass asymmetry μ_A for individual projectiles. This confirms the findings of Singh *et al.* [24], who claimed that Morgenstern's mass asymmetry systematics is valid only for individual projectile(s). Further, a strong dependence of the incomplete fusion strength function (F_{ICF}) on the Coulomb effect, i.e., $Z_P Z_T$ was observed on comparing systems available in literature. It may be interesting if the measurements involving the same CN for different projectile-target combinations is applied, which may give insight to Coulomb effects.

ACKNOWLEDGMENTS

The authors thank the Director of the Inter University Accelerator Center (IUAC), New Delhi, India for extending experimental facilities, and the Pelletron crew to provide us with the stable beams during this experiment. One of the authors (A.Y.) also thanks the DST for providing support through Young Scientist Scheme under startup research Grant No. SB/FTP/PS-194/2013.

[1] P. P. Singh *et al.*, Phys. Lett. B **671**, 20 (2009), and the references therein.
[2] P. R. S. Gomes, I. Padron, E. Crema, O. A. Capurro, J. O. Fernandez Niello, A. Arazi, G. V. Marti, J. Lubian, M. Trotta, A. J. Pacheco, J. E. Testoni, M. D. Rodriguez, M. E. Ortega, L. C. Chamon, R. M. Anjos, R. Veiga, M. Dasgupta, D. J. Hinde, and K. Hagino, Phys. Rev. C **73**, 064606 (2006).
[3] E. Z. Buthelezi *et al.*, Nucl. Phys. A **734**, 553 (2004).
[4] A. Yadav *et al.*, Phys. Rev. C **85**, 064617 (2012); **85**, 034614 (2012).
[5] P. R. S. Gomes, R. Linares, J. Lubian, C. C. Lopes, E. N. Cardozo, B. H. F. Pereira, and I. Padron, Phys. Rev. C **84**, 014615 (2011).
[6] D. J. Hinde and M. Dasgupta, Phys. Rev. C **81**, 064611 (2010).
[7] P. P. Singh, A. Yadav, D. P. Singh, U. Gupta, M. K. Sharma, R. Kumar, D. Singh, R. P. Singh, S. Muralithar, M. A. Ansari, B. P. Singh, R. Prasad, and R. K. Bhowmik, Phys. Rev. C **80**, 064603 (2009).
[8] U. Gupta *et al.*, Nucl. Phys. A **811**, 77 (2008); Phys. Rev. C **80**, 024613 (2009).
[9] P. P. Singh *et al.*, Eur. Phys. J. A **34**, 29 (2007).
[10] V. R. Sharma, A. Yadav, P. P. Singh, D. P. Singh, S. Gupta, M. K. Sharma, I. Bala, R. Kumar, S. Murlithar, B. P. Singh, and R. Prasad, Phys. Rev. C **89**, 024608 (2014).
[11] A. Diaz-Torres, D. J. Hinde, J. A. Tostevin, M. Dasgupta, and L. R. Gasques, Phys. Rev. Lett. **98**, 152701 (2007), and the references therein.
[12] H. C. Britt and A. R. Quinton, Phys. Rev. **124**, 877 (1961).
[13] J. Wilczynski, K. Siwek-Wilczynska, J. vanDriel, S. Gonggrijp, D. C. J. M. Hageman, R. V. F. Janssens, J. Lukasiak, and R. H. Siemssen, Phys. Rev. Lett. **45**, 606 (1980); J. Wilczynski *et al.*, Nucl. Phys. A **373**, 109 (1982).
[14] T. Udagawa and T. Tamura, Phys. Rev. Lett. **45**, 1311 (1980).
[15] J. R. Wu and I. Y. Lee, Phys. Rev. Lett. **45**, 8 (1980).
[16] J. R. Wu, C. C. Chang, and H. D. Holmgren, Phys. Rev. Lett. **40**, 1013 (1978); Phys. Rev. C **19**, 370 (1979).
[17] I. M. Brancus, H. Rebel, J. Wentz, and V. Corcalciuc, Phys. Rev. C **42**, 2157 (1990).
[18] J. P. Bondrof *et al.*, Nucl. Phys. A **333**, 285 (1980).
[19] C. Gerschel, Nucl. Phys. A **387**, 297 (1982).
[20] I. Tserruya *et al.*, Rev. Lett. **60**, 14 (1988).
[21] P. R. S. Gomes *et al.*, Braz. J. Phys. **34**, 737 (2004).
[22] D. J. Parker, J. J. Hogan, and J. Asher, Phys. Rev. C **39**, 2256 (1989).
[23] V. R. Sharma *et al.*, EPJ Web Conf **86**, 00046 (2015).
[24] P. P. Singh *et al.*, EPJ Web Conf. **21**, 10009 (2012).
[25] V. R. Sharma *et al.*, Nucl. Phys. A **946**, 182 (2016).
[26] V. R. Sharma *et al.*, J. Phys. G: Nucl. Part. Phys. **42**, 055113 (2015).
[27] H. Morgenstern, W. Bohne, W. Galster, K. Grabisch, and A. Kyanowski, Phys. Rev. Lett. **52**, 1104 (1984); H. M. Morgenstern *et al.*, Phys. Lett. B **113**, 463 (1982).
[28] The Stopping and Range of Ions in Matter (SRIM) code, http://www.srim.org/SRIM/SRIMLEGL.htm.
[29] B. P. Singh, M. G. V. Sankaracharyulu, M. A. Ansari, H. D. Bhardwaj, and R. Prasad, Phys. Rev. C **47**, 2055 (1993).
[30] E. Brown and R. B. Firestone, *Table of Isotopes* (Wiley, New York, 1986).
[31] A. Gavron, Phys. Rev. C **21**, 230 (1980).
[32] R. Bass, Nucl. Phys. A **231**, 45 (1985).
[33] F. D. Becchetti and G. W. Greenlees, Phys. Rev. **182**, 1190 (1969).
[34] G. R. Satchler, Nucl. Phys. **70**, 177 (1965).
[35] A. Gilbert and A. G. N. Cameron, Can. J. Phys. **43**, 1446 (1965).
[36] H. H. Gutbrod, W. G. Winn, and M. Blann, Phys. Rev. Lett. **30**, 1259 (1973).
[37] P. R. S. Gomes *et al.*, Phys. Lett. B **601**, 20 (2004).
[38] L. R. Gasques, D. J. Hinde, M. Dasgupta, A. Mukherjee, and R. G. Thomas, Phys. Rev. C **79**, 034605 (2009).
[39] A. C. Berriman, D. J. Hinde, M. Dasgupta, C. R. Morton, R. D. Butt, and J. O. Newton, Nature (London) **413**, 144 (2001).
[40] J. P. Lestone, Nucl. Phys. A **559**, 277 (1993).
[41] D. P. Singh, Unnati P. P. Singh, A. Yadav, M. K. Sharma, B. P. Singh, K. S. Golda, R. Kumar, A. K. Sinha, and R. Prasad, Phys. Rev. C **81**, 054607 (2010).
[42] P. P. Singh *et al.*, Phys. Rev. C **78**, 017602 (2008).
[43] P. P. Singh, B. P. Singh, M. K. Sharma, Unnati, D. P. Singh, R. Prasad, R. Kumar, and K. S. Golda, Phys. Rev. C **77**, 014607 (2008), and references therein.
[44] M. Shuaib *et al.*, Phys. Rev. C **94**, 014613 (2016).